Th-MOF showing six-fold imide-sealed pockets for middle-size-separation of propane from nature gas

Feng Luo (ecitluofeng@163.com)
East China University of Technology https://orcid.org/0000-0001-6380-2754
Li Wang
East China University of Technology
Lele Gong
East China University of Technology
Wansheng Jia
East China University of Technology
Rajamani Krishna
University of Amsterdam https://orcid.org/0000-0002-4784-8530
Youyuan Ran
East China University of Technology
Lan Chen
East China University of Technology

Article

Keywords: propane, natural gas, separation mechanism

Posted Date: September 24th, 2021

DOI: https://doi.org/10.21203/rs.3.rs-888730/v1

Abstract

Separation of propane from nature gas is of great importance to industry. However, in light of size-based separation, there still lacks effective method to directly separate propane from nature gas, due to the comparable physical properties for these light alkanes (C1-C4) and the middle size of propane. In this work, we found that a new Th-MOF could be an ideal solution for this issue. The Th-MOF takes UiO-66-type structure, but with the pocket sealed by six-fold imide groups; this not only precisely reduces the size of pocket to exactly match propane, but also enhances the host-guest interactions through multiple supramolecular interactions. As a result, highly selective adsorption of propane over methane, ethane, and butane was observed, implying unique middle-size separation. The actual separation was confirmed by breakthrough experiments, and it is found that both relatively smaller molecules (methane and ethane) and relatively bigger molecules (butane) break through the Th-MOF column within 10 min/g, whereas propane with middle size can maintain very long retention time up to 80 min/g, strongly suggesting middle-size separation and its superior application in direct separation of propane from nature gas. The separation mechanism, as unveiled by both theoretical calculation and comparative experiments, is due to the six-fold imide-sealed pockets that could effectively distinguish propane from other light alkanes through both size effect and host-guest interactions.

Background

Nature gas (NG) widely exists on the earth, with abundant reserves, such as oilfield gas, gas field gas, mud volcanic gas, coalbed methane and biogenic gas, and so on. It contains both light hydrocarbon and nonhydrocarbon gases. The major component of light hydrocarbon consists of methane (85%), ethane (9%), propane (3%), and butane (1%)[1-5]. Accordingly, propane produced from natural gas is important raw materials for modern industry[8-10]. For example, China's propane consumption in 2019 is 16.57 million tons[11].

The dynamic diameter of methane, ethane, propane, and butane is 3.8 Å, 4.0 Å, 4.2 Å, 4.3 Å, respectively, implying difficult separation for this mixture, due to comparable size[12-15]. But they show different molecule size such as 3.76 Å×3.83 Å×3.99 Å for methane, 4.08 Å×4.29 Å×4.72 Å for ethane, 4.02 Å×4.79 Å×6.20 Å for propane, and 4.02 Å×4.61 Å×7.38 Å for butane. This means that we can separate this mixture through precise design on the pore structure and size. Due to the outstanding importance of propane in the industry, thereby, there demands urgent concern about direct generation of propane from nature gas (mainly quaternary gas mixture of methane, ethane, propane, and butane)[16-20]. However, to enforce this target, there still lacks available MOFs or effective molecular design strategy to match exactly the size of propane. On the other hand, in light of size-based separation that is often designed and employed for separation in the field of MOFs, whatever the dynamic diameter and the molecule size of propane is located at the middle among these mixtures, implying a demand of middle-size separation[21-24]. However, this is seriously restricted for common molecular design and most available

MOFs. To the best of our knowledge, there is still no report about direct separation of propane from nature gas until this work.

The size and configuration of pore in MOFs presents a highly important factor for separation[25-29]. MOFs could selective adsorption of gas molecules with smaller size than the pore MOFs, but will exclude these gas molecules with bigger size than the pore MOFs[30,31]. And co-adsorption would occur when all the components in the gas mixture with smaller size than the pore MOFs; this often leads to weak or no separation[32-34]. Thereby, separation of molecule with middle size among the gas mixture remains a challenging task[35,36]. Flexible framework with gate opening could be a good resolution. For example, just the target molecule with middle size can result in the gate opening, and other molecules with relatively smaller size or bigger size could not result in the gate opening, consequently leading to selective adsorption of middle-size molecule. This unique phenomenon has been realized by Zhang *et al* for separation of styrene from ethylbenzene/styrene/ toluene/benzene mixture[37]. However, this type separation is highly dependent on the magnitude of host-guest interactions, thus, restricting its application for other mixtures.

Anchoring functionalized units on the pore wall of MOFs to enhance the host-guest interactions is also an effective method for separation[38-40]. This can theoretically selectively adsorb target molecule from the mixture under precise design on the functionalized units. However, this method could be also invalid to perform middle-size separation for these molecules with similar structure and physical properties.

In this work, we found that the combination of size control and anchoring functionalized units is an effective solution to give middle-size separation for propane from nature gas (see Scheme 1). The used MOF show the pore size bigger than methane, ethane, and propane, but less than butane, and the pore wall is decorated by three-fold imide groups that acts as strong H-acceptor for enhance host-guest interactions. Selective adsorption of propane over methane and ethane is due to the relatively stronger host-guest interactions between propane and MOFs, while selective adsorption of propane over butane is due to the big size of butane (relative to the pore of MOF).

Results

Synthesis, crystal structure, and characterization of ECUT-Th-10. The MOF, namely **ECUT-Th-10**, was synthesized by the solvothermal reaction of $Th(NO_3)_4$, N,N'-bis-(4-benzoic acid)-1,4,5,8-naphthalenediimide (H_2L) and perchloric acid. Light orange octahedral crystal was obtained. The purity of the as-synthesized samples was confirmed by PXRD tests (Supplementary Fig. 1). The synthetic details of the ligand H_2L and MOF was presented in the supporting information. Single-crystal X-ray diffraction analysis shows that **ECUT-Th-10** crystallizes in the cubic space group *Fd-3m* with big unit cell of $a=b=c$=39.5857(7) Å and large volume of 62032(3) $Å^3$ (Supplementary Table 1). The asymmetric unit contains one crystallography-independent Th (IV), which is coordinated by four carboxylate oxygen atoms from four different L^{2-} ligands, two μ^3-OH ions, and two μ^3-O^{2-} ions, forming a square antiprismatic

geometry (Fig. 1b). The Th-O bonds are in the normal range, comparable with that observed in the literature. The L^{2-} ligands afford the bidentate mode to connect to four Th (IV) ions. Due to steric hindrance, the middle imide-containing fragment is rotated and show almost vertical to the two terminal benzene rings, as evidenced by the dihedral angle of 88.97º and 88.53º between them (Fig. 1a).

Through μ^3-OH ions and μ^3-O^{2-} ions, six identical Th(IV) ions are integrated to generate a $Th_6(\mu^3\text{-}OH)_4(\mu^3\text{-}O^{2-})_4$ building block, which is very similar with the well-known $Zr_6(\mu^3\text{-}OH)_4(\mu^3\text{-}O^{2-})_4$ building block in UiO-66-type structures. Each $Th_6(\mu^3\text{-}OH)_4(\mu^3\text{-}O^{2-})_4$ core connects to twelve L^{2-} ligands, and an overall UiO-66-type structure is observed in **ECUT-Th-10** (Fig. 1c). Interestingly, as observed in UiO-66, **ECUT-Th-10** also affords two different cages of octahedral and tetrahedral cages. However, the octahedral cage is as large as to 2.6 nm, due to the use of long ligand of L^{2-} (Fig. 1d). The tetrahedral cage in **ECUT-Th-10** is divided into two types of pores, and four three-fold imide-sealed pockets are observed at the vertex of tetrahedral cage that gives the aperture of 6.1 Å (Fig. 1e); this is impressively matchable with the size of propane, but bigger than methane and ethane, and smaller than butane, implying its potential for selective adsorption of propane over methane, ethane, and butane, finally leading to middle-size separation. However, UiO-66 just shows one type of pore for tetrahedral cage with size about 8 Å (Fig. 1f). The formation of unique three-fold imide-sealed pockets in **ECUT-Th-10** is due to the use of L^{2-} ligands that show the rotation of imide-containing fragment and results in a vertical configuration for the L^{2-} ligand between the middle imide-containing fragment and two terminal benzene rings, and finally cause the imide C=O bonds to orient inside the tetrahedral cage. Notably, two-fold interpenetration is observed in **ECUT-Th-10**, which largely reduces the pore. And the three-fold imide-sealed pockets is then further sealed by additional three imide units from another net, constructing the overall six-fold imide-sealed pockets (Fig. 1g).

To confirm the permanent porosity, we first carried out thermogravimetric analysis (TGA) of **ECUT-Th-10**, showing that the guest molecules can be removed before 250 ℃ (Supplementary Fig. 2). But this can be decreased through CH_3OH treatment, since the CH_3OH-exchanged samples showed the solvent loss before 100℃. Therefore, the activation of **ECUT-Th-10** was prepared at 100℃ under vacuum. To check the porosity, N_2 adsorption-desorption behavior was studied at 77 K. As shown in Fig. 2a, the uptake capacity of N_2 is around 250 cm^3/g at 1 bar. The Brunauer–Emmett–Teller (BET) surface area was calculated to be 854 m^2/g. The size distribution gives a narrow pore at 0.63 nm and broad pore at 1.3 nm, where the narrow pore belongs to the six-fold imide-sealed pockets and the broad pore belongs to the reduced pore (such as the pristine large octahedral cage) due to interpenetration.

Gas adsorption and separation performances. The above results further motivate us to investigate its application in separation of nature gas. First, the single component isotherms of CH_4, C_2H_6, C_3H_8 and n-C_4H_{10} were measured at 298 K, respectively (Fig. 2b). The uptake at 298 K and 110 kPa is respectively 2.89 mmol/g (C_3H_8), 2.69 mmol/g (C_4H_{10}), 1.72 mmol/g (C_2H_6), and 0.42 mmol/g (CH_4), suggesting selective adsorption of propane over methane, ethane, and butane. Especially, no adsorption

for C_4H_{10} at low pressure before 13 kPa is observed, implying that butane is excluded from **ECUT-Th-10** under this condition, since the size of butane is bigger than the pore size of six-fold imide-sealed pockets. As for methane, ethane, and propane, similar phenomenon is not observed, because their sizes are smaller than the pore size of six-fold imide-sealed pockets. Thereby, the adsorption ratio at low pressure (13 kPa) is as high as to 30 for C_3H_8/C_4H_{10}, 3.75 for C_3H_8/C_2H_6, and 17.1 for C_3H_8/CH_4, strongly indicative of selective adsorption towards propane. The sharp increase after 13 kPa observed in the adsorption isotherm for butane is mainly resulted from gate opening, owning to somewhat flexibility of the MOF framework. Gate opening is often encountered in MOFs and is generally used for separation[41-43].

The adsorption selectivity is also evaluated by ideal adsorption solution theory (IAST), in light of the above single component isotherms at 298 K (Fig. 2c) [44-47]. Ultrahigh selectivity up to 60 for C_3H_8/C_4H_{10} (50:50 v/v), 9.31 for C_3H_8/C_2H_6 (50:50 v/v), and 54.5 for C_3H_8/CH_4 (50:50 v/v) is respectively observed at the onset of adsorption, also suggesting selective adsorption of propane.

We further investigated the host-guest interaction between **ECUT-Th-10** and these gases, which is mainly reflected on the isosteric heat of adsorption (Q_{st}). Thus, the adsorption of these gases at 273 K was carried out (Supplementary Fig. 3). Due to gate opening in C_4H_{10}, its fitting of the adsorption isotherms at 298 K cannot obtain reasonable value, thus its Q_{st} value cannot be estimated. The Q_{st} value for other gases gives the hierarchy of C_3H_8 (33.6 kJ/mol) > C_2H_6 (27.3 kJ/mol) > CH_4 (26.4 kJ/mol), implying stronger host-guest interactions for propane (Fig. 2d).

To evaluate the actual separation ability of **ECUT-Th-10** in nature gas, we further carried out breakthrough experiments at 298 K. Initially, we investigated the separation of the equimolar C_3H_8 and C_2H_6 mixtures (50:50, v/v), as both of them holds closer molecule size and smaller size than the pore of six-fold imide-sealed pockets that means inevitable co-adsorption and consequently weak or no separation. As shown in Fig. 2e, C_2H_6 was first eluted though the bed within 32 min/g, whereas C_3H_8 break through after 70 min/g, clearly showing separation of C_3H_8 from C_3H_8/C_2H_6 mixture. To confirm this, we repeated the experiments twice, and repeatable results were observed, also suggesting excellent recyclability for the present MOF adsorbent (Supplementary Fig. 4). Then, equimolar 3-component $CH_4/C_2H_6/C_3H_8$ mixture is measured, where all the components show smaller size than the pore of six-fold imide-sealed pockets (Fig. 2f). Notably, clearly separation for C_3H_8 is also observed, as evidenced by the sequence of outgoing gas such as 10 min/g for CH_4, 20 min/g for C_2H_6, and 48 min/g for C_3H_8. Furthermore, we also measured the equimolar 3-component $C_2H_6/C_3H_8/C_4H_{10}$ mixture, where C_4H_{10} shows bigger size than the pore of six-fold imide-sealed pockets. As expected, C_3H_8 can be also completely separated from this mixture, and the retention time for C_2H_6 and C_4H_{10} is about 10 min/g and the corresponding value for C_3H_8 is as long as 42 min/g (Fig. 2g). Finally, we carried out the breakthrough experiments with equimolar quaternary $CH_4/C_2H_6/C_3H_8/C_4H_{10}$ mixture at 298 K and the results are shown in Fig. 2h. It is impressive that middle-size separation of C_3H_8 from this quaternary mixture is observed, and very long retention time up to 83

min/g is observed for C_3H_8, while CH_4, C_2H_6, and C_4H_{10} just render short retention time within 15 min/g, implying excellent separation of C_3H_8 from this quaternary mixture. The results suggest its superior application for direct separation of propane from nature gas.

To disclose the separation mechanism, we further carried on additionally comparative experiment and DFT (density functional theory) calculation. Due to the high similarity of our MOF with UiO-66 in the structural aspect, in conjunction with the difference in the aspect of tetrahedral cage, UiO-66 is selected to give a comparative research. UiO-66 was synthesized by solvothermal method[48]. The purity of the as-synthesized UiO-66 was confirmed by PXRD tests (Supplementary Fig. 5). The tetrahedral cage in UiO-66 is about 8 Å, which is bigger than the molecular size of methane, ethane, propane, and butane. Accordingly, middle-size separation is not expected for UiO-66. Then, we first tested the single component isotherms of CH_4, C_2H_6, C_3H_8 and n-C_4H_{10} at 298 K, respectively, giving the adsorption capacity in the hierarchy of n-C_4H_{10} (4.5 mmol/g) > C_3H_8 (4.0 mmol/g) > C_2H_6 (2.3 mmol/g) > CH_4 (0.5 mmol/g) (Fig. 3a). The results means that the adsorption capacity of these gases increases along with increasing molecular size of gas molecules, completely excluding the selective adsorption of middle-size molecule as observed in **ECUT-Th-10**. Gate opening in UiO-66 is also not observed for butane, since it affords bigger tetrahedral cage than the molecular size of butane. Moreover, the corresponding C_3H_8/C_4H_{10}, C_3H_8/C_2H_6 and C_3H_8/CH_4 adsorption selectivity was also calculated, giving S=0.4, 2.0 and 32 at the onset of adsorption, respectively (Fig. 3b). This value is fairly less than that observed in our MOF such as S=60, 9.31, and 54.5, respectively, which is mainly due to the reduced size and enhanced host-guest interactions from the six-fold imide-sealed pockets in **ECUT-Th-10**. The adsorption ratio at 13 kPa in UiO-66 is 0.65 for C_3H_8/C_4H_{10}, 1.93 for C_3H_8/C_2H_6, 26.15 for C_3H_8/CH_4, indicative of the hard propane extraction (Fig. 3c). The absence of middle-size separation was further confirmed by breakthrough experiments from the equimolar quaternary $CH_4/C_2H_6/C_3H_8/C_4H_{10}$ mixture at 298 K, where the breakthrough sequence also obeys the order of molecular size (Fig. 3d). In light of these comparative experiment results, we can reason the mechanism of middle-size separation in **ECUT-Th-10** from the unique six-fold imide-sealed pockets that gives matchable size and enhanced host-guest interactions with propane over other gases such as methane, ethane, and butane.

Mechanism of gas adsorption by theoretical calculations. To obtain the structural information after adsorption of gas molecules, we then carried out DFT calculation. It is found that the adsorption of these gas molecules is primarily located at six-fold imide-sealed pockets. And each pocket could accommodate one molecule. The calculated binding energies between these gas molecules and the six-fold imide-sealed pocket are -9.65 kJ/mol (CH_4), -17.38 kJ/mol (C_2H_6), -24.12 kJ/mol (C_3H_8), 11.58 kJ/mol (C_4H_{10}), respectively. This means that the adsorption of CH_4, C_2H_6, and C_3H_8 is thermodynamically spontaneous, owing to their molecular size less than the pore of the six-fold imide-sealed pocket, whereas the positive binding energy indicates that the adsorption of C_4H_{10} is excluded, due to its molecular size bigger than the pore of the six-fold imide-sealed pocket; this is well consistent with the experimental results. In addition, it is found that C_3H_8 in the six-fold imide-sealed pocket is tightly fixed by multiple

hydrogen bonds from imide units with C-H•••O distance of 3.29 (3) Å-4.02(3) Å (Fig. 4b). By contrast, weak hydrogen bonds are observed for CH_4 with distance of 4.19(3) Å-4.31(3) Å and C_2H_6 with distance of 3.35(3) Å-4.15(3) Å (Supplementary Fig. 6 and Fig. 7). Thereby, supramolecular interactions from the imide units enhancing the host-guest interaction for C_3H_8 is also responsible for the middle-size separation.

Discussion

In summary, we reported a novel MOF, **ECUT-Th-10,** which holds the UiO-66-type structure, but is constructed by diimide-based ligands and enables an interpenetrated structure with the formation of unique six-fold imide-sealed pockets. These structural merits are beneficial to separate propane from methane/ethane/propane/butane mixture, demonstrated an extremely rare case of middle-size separation, suggesting its big potential in direct generation of propane from nature mixture. The pocket-like cage exhibited an excellent molecular sieving effect to block larger C_4H_{10}, while imide units within this pocket-like cage provide multiple supramolecular interactions with propane, thus enhancing the host-guest interactions for propane, consequently reducing the co-adsorption for methane, ethane, and propane and performing highly selective adsorption towards propane.

References

[1] Zhang, Y., Yang, L., Wang, L., Cui, X. & Xing. H. Pillar iodination in functional boron cage hybrid supramolecular frameworks for high performance separation of light hydrocarbons. *J. Mater. Chem. A.* **7**, 27560–27566 (2019).

[2] Wu, Y., Sun, Y., Xiao, J., Wang, X. & Li, Z. Glycine-modified HKUST-1 with simultaneously enhanced moisture stability and improved adsorption for light hydrocarbons separation. *ACS Sustainable Chem. Eng*. **7**, 1557–1563 (2019).

[3] Wang, J., Krishna, R., Yang, T. & Deng. S. Nitrogen-rich microporous carbons for highly selective separation of light hydrocarbons. *J. Mater. Chem. A.* **4**, 13957–13966 (2016).

[4] He, Y., Krishna, R. & Chen. B. Metal–organic frameworks with potential for energy-efficient adsorptive separation of light hydrocarbons. *Energy Environ. Sci.* **5**, 9107–9120 (2012).

[5] Peng, Y. L. et al. A robust heterometallic ultramicroporous MOF with ultrahigh selectivity for propyne/propylene separation. *J. Mater. Chem. A.* **9**, 2850–2856 (2021).

[6] Borah, B., Zhang, H. & Snurr. R. Q. Diffusion of methane and other alkanes in metal-organic frameworks for natural gas storage. *Chem. Eng. Sci.* **124**, 135–143 (2015).

[7] Wu, Y. & Weckhuysen, B. M. Separation and purification of hydrocarbons with porous materials. *Angew. Chem. Int. Ed*. **60**, 18930–18949 (2021).

[8] Wang, Y. et al. Solvent-induced framework-interpenetration isomers of Cu MOFs for efficient light hydrocarbon separation. *Inorg. Chem. Front.* **5**, 2408–2412 (2018).

[9] Li, L., Yin, Q., Li, H. F., Liu, T. F. & Cao. R. Rational design of phosphonocarboxylate metal–organic frameworks for light hydrocarbon separations. *Mater. Chem. Front.* **2**, 1436–1440 (2018).

[10] Chen, Y. et al. Selective adsorption of light alkanes on a highly robust indium based metal–organic framework. *Ind. Eng. Chem. Res.* **56**, 4488–4495 (2017).

[11] https://wenku.baidu.com/view/ef04309029160b4e767f5acfa1c7aa00b42a9d68.html.

[12] Geng, D. et al. A 2D metal–thiacalix[4]arene porous coordination polymer with 1D channels: gas absorption/separation and frequency response. *Dalton Trans.* **47**, 9008–9013 (2018).

[13] Zheng, B., Pan, Y. C., Lai, Z. P. & Huang, K. W. Molecular dynamics simulations on gate opening in ZIF-8: identification of factors for ethane and propane separation. *Langmuir* **29**, 8865–8872 (2013).

[14] Li, J. R., Kuppler, R. J. & Zhou, H. C. Selective gas adsorption and separation in metal–organic frameworks. *Chem. Soc. Rev.* **38**, 1477–1504 (2009).

[15] Lin. J. Y. S. Molecular sieves for gas separation. *Science* **353**,121–122 (2016).

[16] Kan, L., Li, G. & Liu. Y. Highly selective separation of C_3H_8 and C_2H_2 from CH_4 within two water-stable Zn5 cluster-based metal–organic frameworks. *ACS Appl. Mater. Interfaces* **12**, 18642–18649 (2020).

[17] Shi, R. et al. Highly selective adsorption separation of light hydrocarbons with a porphyrinic zirconium metal-organic framework PCN-224. *Sep. Purif. Technol.* **207**, 262–268 (2018).

[18] Wang, Y. et al. Selective aerobic oxidation of a metal–organic framework boosts thermodynamic and kinetic propylene/propane selectivity. *Angew. Chem. Int. Ed.* **131**, 7774–7778 (2019).

[19] Cadiau, A., Adil, K., Bhatt, P. M., Belmabkhout, Y. & Eddaoudi. M. A metal-organic framework–based splitter for separating propylene from propane. *Science* **353**, 137–140 (2016).

[20] Zeng, H. et al. Orthogonal-array dynamic molecular sieving of propylene/propane mixtures. *Nature* **595**, 542–549 (2021).

[21] Bao, Z. et al. Potential of microporous metal–organic frameworks for separation of hydrocarbon mixtures. *Energy Environ. Sci.* **9**, 3612–3641 (2016).

[22] Cui, W. G., Hu, T. L. & Bu. X. H. Metal–organic framework materials for the separation and purification of light hydrocarbons. *Adv. Mater.* **32**, 1806445 (2020).

[23] Wang, Y. & Zhao. D. Beyond equilibrium: metal–organic frameworks for molecular sieving and kinetic gas separation. *Cryst. Growth Des.* **17**, 2291–2308 (2017).

[24] Li, J. R., Kuppler, R. J. & Zhou. H. C. Selective gas adsorption and separation in metal–organic frameworks. *Chem. Soc. Rev.* **38**, 1477–1504 (2009).

[25] Furukawa, S., Reboul, J., Diring, S., Sumida, K. & Kitagawa, S. Structuring of metal–organic frameworks at the mesoscopic/macroscopic scale. *Chem. Soc. Rev.* **43**, 5700–5734 (2014).

[26] Adil, K. et al. Gas/vapour separation using ultra-microporous metal–organic frameworks: insights into the structure/separation relationship. *Chem. Soc. Rev.* **46**, 3402–3430 (2017).

[27] Duan, J., Pan, Y., Liu, G. & Jin. W. Metal-organic framework adsorbents and membranes for separation applications. *Curr. Opin. Chem. Eng.* **20**, 122–131 (2018).

[28] Ying, Y. et al. Pressure-responsive two-dimensional metal-organic framework composite membranes for CO_2 separation. *Angew. Chem. Int. Ed*. **133**, 11419–11426 (2021).

[29] Wang, Y. et al. One-step ethylene purification from an acetylene/ethylene/ethane ternary mixture by cyclopentadiene cobalt-functionalized metal–organic frameworks. *Angew. Chem. Int. Ed.* **60**, 11350–11358 (2021).

[30] Li, B. et al. An ideal molecular sieve for acetylene removal from ethylene with record selectivity and productivity. *Adv. Mater.* **29**,1704210 (2017).

[31] Assen, A. H. et al. Tunable rare earth fcu-MOF platform: access to adsorption kinetics driven gas/vapor separations via pore size contraction. *Angew. Chem. Int. Ed.* **54**, 14353–14358 (2015).

[32] Hamon, L. et al. Co-adsorption and separation of CO_2–CH_4 mixtures in the highly flexible MIL-53(Cr) MOF. *J. Am. Chem. Soc.* **131**, 17490–17499 (2009).

[33] Lin, R. B. et al. Molecular sieving of ethylene from ethane using a rigid metal-organic framework. *Nat. Mater.* **17,** 1128–1133 (2018).

[34] Liang, B. et al. An ultramicroporous metal–organic framework for high sieving separation of propylene from propane. *J. Am. Chem. Soc.* **142**, 17795–17801 (2020).

[35] Zhang, Z. et al. Sorting of C4 olefins with interpenetrated hybrid ultramicroporous materials by combining molecular recognition and size-sieving. *Angew. Chem. Int. Ed*. **56**, 16282–16287 (2017).

[36] Ding, Q. et al. Exploiting equilibrium-kinetic synergetic effect for separation of ethylene and ethane in a microporous metal-organic framework. *Sci. Adv*. **6**, eaaz4322 (2020).

[37] Zhou, D. D. et al. Intermediate-sized molecular sieving of styrene from larger and smaller analogues. *Nat. Mater.* **18**, 994–999 (2019).

[38] Chen, X. et al. Direct observation of Xe and Kr adsorption in a Xe-selective microporous metal–organic framework. *J. Am. Chem. Soc.* **137**, 7007–7010 (2015).

[39] Gan, L. et al. A Highly water-stable meta-carborane-based copper metal–organic framework for efficient high-temperature butanol separation. *J. Am. Chem. Soc*. **142**, 8299–8311 (2020).

[40] Li, L. et al. A robust squarate-based metal–organic framework demonstrates record-high affinity and selectivity for xenon over krypton. *J. Am. Chem. Soc.* **141**, 9358–9364 (2019).

[41] Roztocki, K. et al. Collective breathing in an eightfold interpenetrated metal-organic framework: from mechanistic understanding towards threshold sensing architectures. *Angew. Chem. Int. Ed.* **132**, 4521–4527 (2020).

[42] Yang, H. et al. Lock-and-Key and shape-memory effects in an unconventional synthetic path to magnesium metal–organic frameworks. *Angew. Chem. Int. Ed*. **58**, 11757–11762 (2019).

[43] Taylor, M. K. et al. Tuning the adsorption-induced phase change in the flexible metal–organic framework Co(bdp). *J. Am. Chem. Soc.* **138**, 15019–15026 (2016).

[44] Luo, F. et al. UTSA-74: A MOF-74 isomer with two accessible binding sites per metal center for highly selective gas separation. *J. Am. Chem. Soc*. **138**, 5678–5684 (2016).

[45] Yin, M. et al. A [Th_8Co_8] nanocage-based metal–organic framework with extremely narrow window but flexible nature enabling dual-sieving effect for both isotope and isomer separation. *CCS Chem*. **3**, 1115–1126 (2021).

[46] Zhang, H. et al. Robust metal–organic framework with multiple traps for trace Xe/Kr separation. *Sci. Bull.* **66**, 1073–1079 (2021).

[47] Wang, L. et al. Constructing redox-active microporous hydrogen-bonded organic framework by imide-functionalization: Photochromism, electrochromism, and selective adsorption of C_2H_2 over CO_2. *Chem. Eng. J.* **383**, 123117 (2020).

[48] Cavka, J. H. et al. A new zirconium inorganic building brick forming metal organic frameworks with exceptional stability. *J. Am. Chem. Soc.* **130**, 13850–13851 (2008).

Declarations

Acknowledgements

We thanks to Open Fund of Jiangxi Province Key Laboratory of Synthetic Chemistry (JXSC202007), Doctoral Scientific Research Start-up Foundation of East China University of Technology (DHBK2018044), the National Natural Science Foundations of China (21966002, 21871047), the Training

Program for Academic and Technical Leaders of Major Disciplines in Jiangxi Province (20194BCJ22010), and the Fuzhou youth leading talent project (2020ED64).

Author contributions

F. Luo and L. Wang conceived the experiments and wrote this paper; W. Jia, Y. Ran and L. Chen did experiments; L. Gong carried out computational simulations; R. Krishna calculated the selectivity and Q_{st}.

Additional information

Supplementary Information accompanies this paper at http://www.nature.com/

Competing financial interests

The authors declare no competing financial interest.

Figures

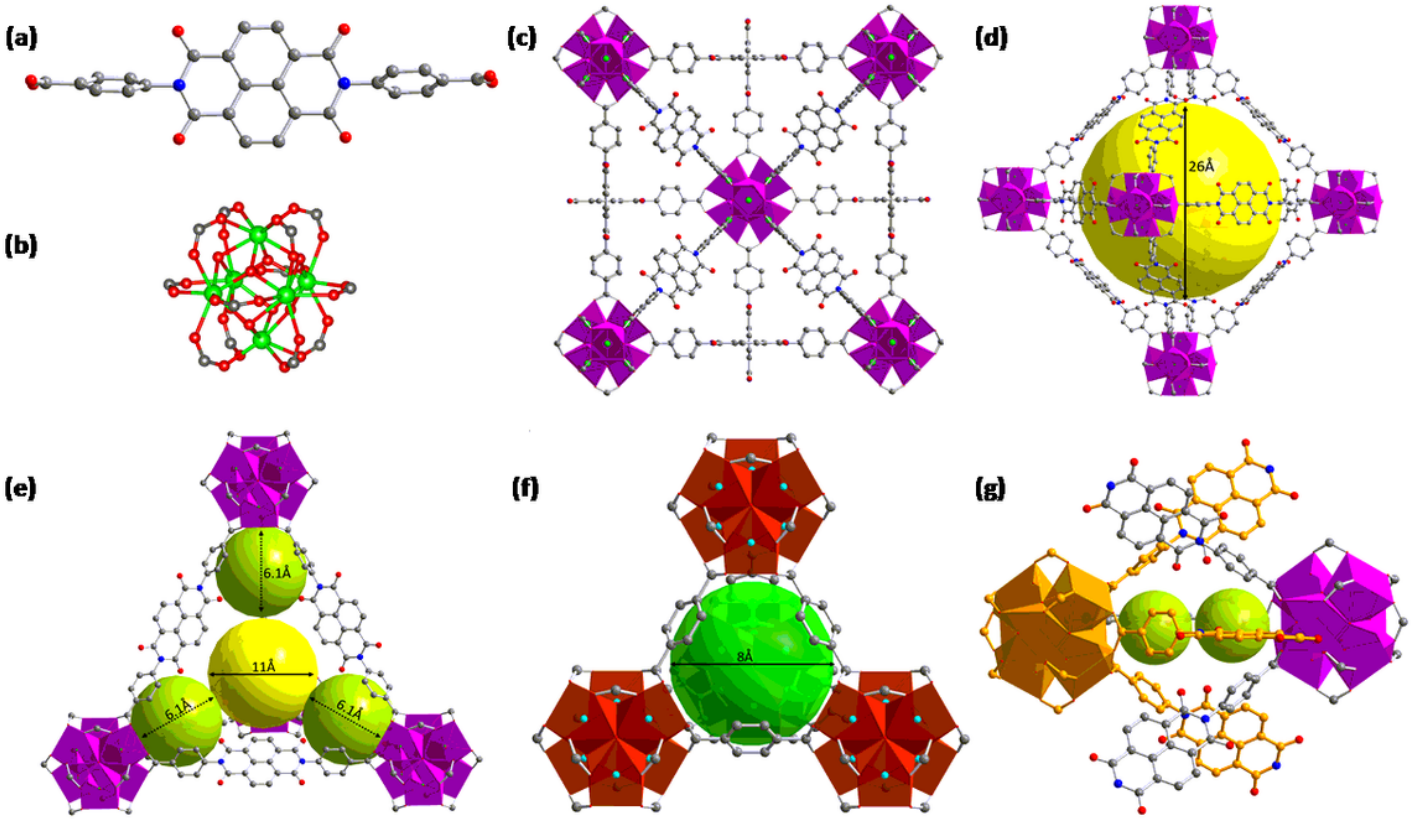

Figure 1

The structure of ECUT-Th-10. (a) The ligand H2L. (b) The Th6(μ3-OH)4(μ3-O2-)4 building block. (c) The UiO-66-type structure of ECUT-Th-10. (d) The octahedral cage in ECUT-Th-10. (e) The tetrahedral cage in ECUT-Th-10 with four unique three-fold imide-sealed pockets at the vertex of tetrahedral cage. (f) A comparison of the tetrahedral cage in UiO-66. (g) The unique six-fold imide-sealed pockets formed by interpenetration.

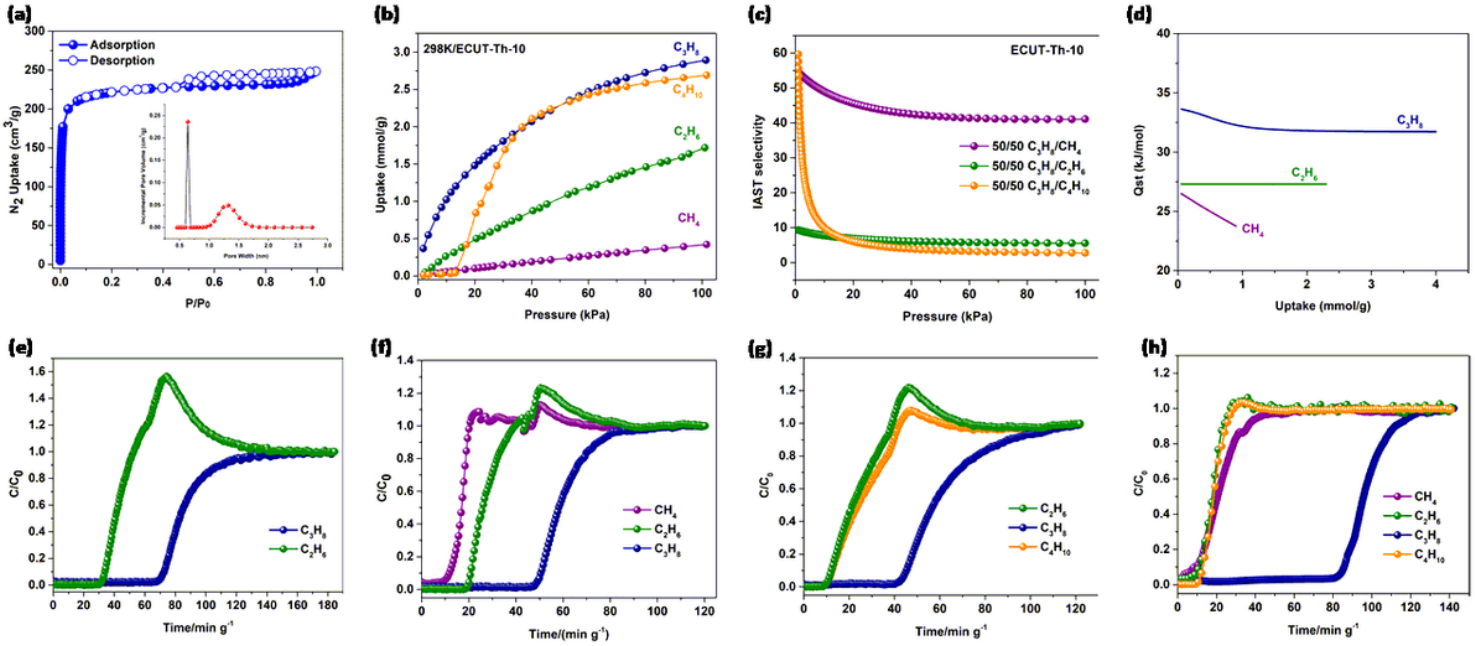

Figure 2

The adsorption and separation research upon ECUT-Th-10. (a) The adsorption isotherm of N2 at 77 K with the insert of pore size distribution. (b) The adsorption isotherms of CH4, C2H6, C3H8 and C4H10. (c) The IAST selectivity of ECUT-Th-10 for different gases. (d) The isosteric heat of adsorption for CH4, C2H6 and C3H8 in ECUT-Th-10. (e) Experimental breakthrough curves for C2H6/C3H8 (50/50, v/v) binary mixture at 298 K. (f) Experimental breakthrough curves for CH4/C2H6/C3H8 (33/33/33, v/v/v) 3-component mixture at 298 K. (g) Experimental breakthrough curves for C2H6/C3H8/C4H10 (33/33/33, v/v/v) 3-component mixture at 298 K. (h) Experimental breakthrough curves for CH4/C2H6/C3H8/C4H10 (25/25/25/25, v/v/v/v) 4-component mixture at 298 K.

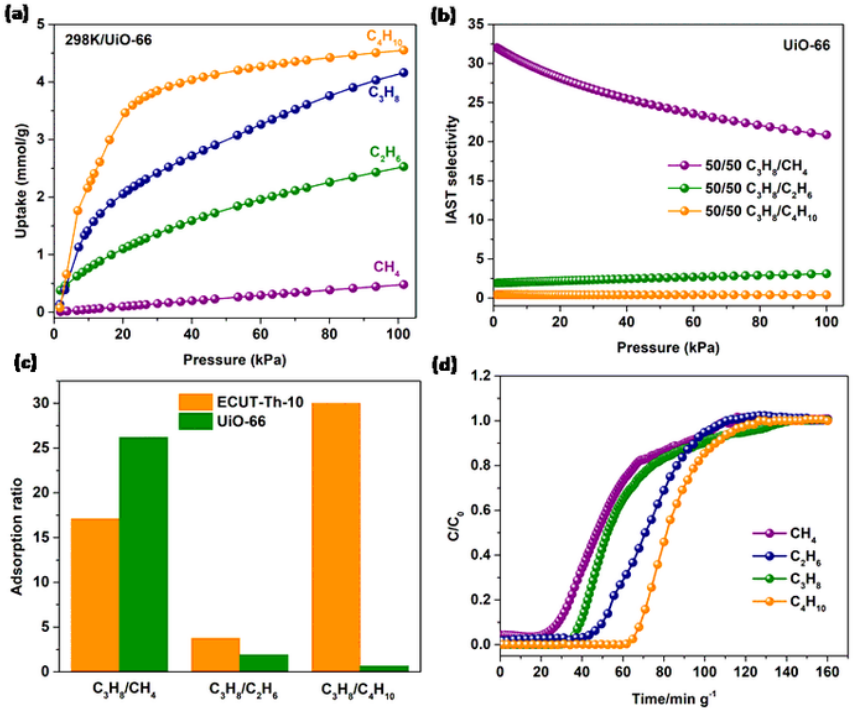

Figure 3

The adsorption and selectivity of UiO-66. (a) The adsorption isotherms of UiO-66 for CH4, C2H6, C3H8 and C4H10. (b) The IAST selectivity data of UiO-66 for different gases. (c) The adsorption ratio for ECUT-Th-10 and UiO-66 at 13 kPa. (d) Experimental breakthrough curves of UiO-66 for CH4/C2H6/C3H8/C4H10 (25/25/25/25, v/v/v/v) 4-component mixture at 298 K.

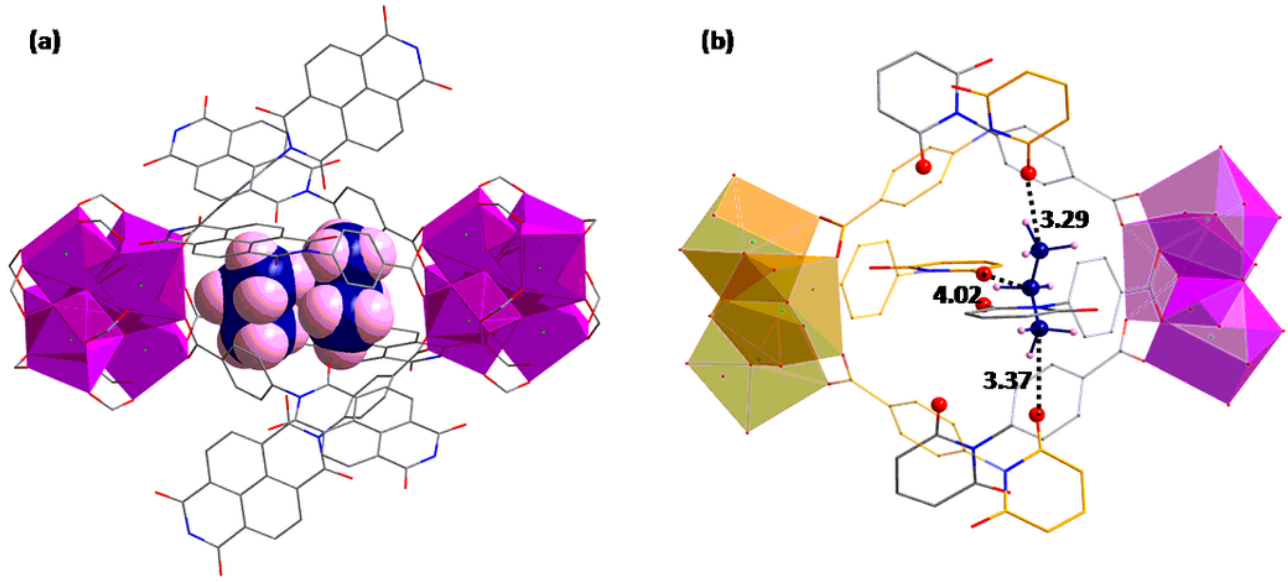

Figure 4

The bonding sites of C3H8 in ECUT-Th-10. (a) The optimal location of C3H8 in the pocket cage. (b) The C-H•••O interaction between C3H8 and the imide units.

Supplementary Files

This is a list of supplementary files associated with this preprint. Click to download.

- ThMOF10.cif
- Supportinginformation.docx
- ThMOF10.cif
- checkcif.pdf